

# THE KRAMERS PROBLEM IN THE ENERGY-DIFFUSION LIMITED REGIME

José M. Sancho

Institute for Nonlinear Science 0402

University of California San Diego

La Jolla, California 92093-0402

and

Departament d'Estructura i Constituents de la Matèria

Universitat de Barcelona

Av. Diagonal 647, E-08028 Barcelona, Spain

Aldo H. Romero

Department of Chemistry and Biochemistry 0340

and Department of Physics

University of California, San Diego

La Jolla, California 92093-0340

Katja Lindenberg

Department of Chemistry and Biochemistry 0340

and Institute for Nonlinear Science

University of California San Diego

La Jolla, California 92093-0340

December 31, 2021

## Abstract

The Kramers problem in the energy-diffusion limited regime of very low friction is difficult to deal with analytically because of the repeated recrossings of the barrier that typically occur before an asymptotic rate constant is achieved. Thus, the transmission coefficient of particles over the potential barrier undergoes oscillatory behavior in time before settling into a steady state. Recently, Kohen and Tannor [D. Kohen and D. J.

Tannor, J. Chem. Phys. **103**, 6013 (1995)] developed a method based on the phase space distribution function to calculate the transmission coefficient as a function of time in the *high-friction* regime. Here we formulate a parallel method for the *low-friction* regime. We find analytic results for the full time and temperature dependence of the rate coefficient in this regime. Our low-friction result at long times reproduces the equilibrium result of Kramers at very low friction and extends it to higher friction and lower temperatures below the turn-over region. Our results indicate that the single most important quantity in determining the entire time evolution of the transmission coefficient is the rate of energy loss of a particle that starts above the barrier. We test our results, as well as those of Kohen and Tannor for the Kramers problem, against detailed numerical simulations.

## 1 Introduction

The classic work of Kramers in 1940 [1] on reaction rates in which the effect of the solvent was taken into account in the form of a Markovian dissipation and Gaussian delta-correlated fluctuations has spawned an enormous and important literature that continues to flourish [2, 3]. Recent advances in experimental methods that make it possible to monitor the progress of chemical reactions on microscopic (even single-molecule single-event) spatial and temporal scales [4, 5] have led to a revival of interest in theoretical approaches that examine the problem on these detailed scales.

The enormous literature on the theoretical front since the appearance of Kramers' seminal paper has evolved in many directions that include more formal derivations of Kramers' own results, extensions to larger parameter regimes and to non-Markovian dissipation models, generalizations to more complex potentials and to many degrees of freedom, analysis of quantum effects, and application to specific experimental systems.

One such recent direction, developed by Kohen and Tannor (KT) [3], deals with the derivation of the rate coefficient in the Kramers problem and in the more general Grote-Hynes problem [6] (that is, the Kramers problem extended to a non-Markovian dissipative memory kernel) so as to obtain not only the asymptotic rate constant but the behavior of the rate coefficient at all times. This derivation is based on the reactive flux method [2, 7, 8]

and allows the interpretation of the salient features of the time dependent rate coefficient  $k(t)$  in terms of the time evolution of the representative distribution functions that originate at the top of the barrier, thus paralleling closely and usefully the methods used in numerical simulations of the problem. KT analyze in detail the dependence on the dissipative memory kernel of the time it takes the rate coefficient to reach its stationary (equilibrium) value. Their extensive analysis, however, does not cover a number of parameter regimes, nor do they check their time-dependent results against numerical simulations. We undertake such studies to complement their work. Thus, we extend the parameter regime of analysis and check some of their results as well as our new ones against numerical simulations.

In this paper we restrict ourselves to the Markovian regime, that is, to the original Kramers problem, deferring the analysis of the non-Markovian case to a subsequent publication. The dynamical equation of interest to us is thus the generic reaction coordinate problem

$$\begin{aligned}\dot{q} &= \frac{p}{m} \\ \dot{p} &= -\gamma p - \frac{dV(q)}{dq} + f(t)\end{aligned}\tag{1}$$

where  $q(t)$  is the time-dependent reaction coordinate, a dot denotes a time derivative,  $\gamma$  is the dissipation parameter,  $V(q)$  is the potential energy, and  $f(t)$  represents Gaussian delta-correlated fluctuations that satisfy the fluctuation-dissipation relation

$$\langle f(t)f(\tau) \rangle = 2\gamma k_B T \delta(t - \tau).\tag{2}$$

$k_B$  is Boltzmann's constant and  $T$  is the temperature. The potential  $V(q)$  is a double-well potential that is often (and here as well) taken to be of the form

$$V(q) = V_0 \left( \frac{q^4}{4} - \frac{q^2}{2} + \frac{1}{4} \right) = \frac{V_0}{4} (q^2 - 1)^2\tag{3}$$

(see Fig. 1). The minima of the potential occur at  $q = \pm 1$ , the potential barrier has a maximum at  $q = 0$ , and the barrier height there is  $V_0/4$ . The parameter  $V_0$  can be used as the unit of energy, and henceforth we set it equal to unity. The barrier height is assumed to

be large compared to the temperature (i.e.,  $k_B T \ll 1/4$ ); otherwise the notion of a barrier crossing process loses its meaning.

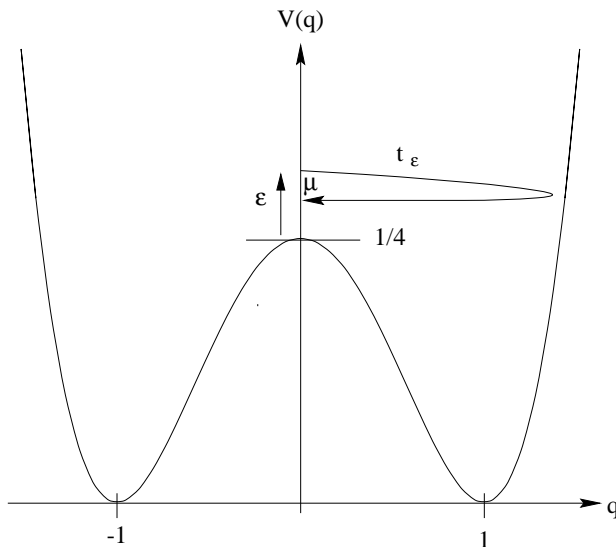


Figure 1: Potential energy for the Kramers problem as given in Eq. (3) with  $V_0 = 1$ . The minima of the potential occur at  $q = \pm 1$ , the maximum at  $q = 0$ , and the barrier height is  $1/4$ .  $\varepsilon$  measures the energy above the barrier,  $t_\varepsilon$  is the time it takes a particle of energy  $\varepsilon$  above the barrier starting at  $q = 0$  to return to  $q = 0$ , and  $\mu$  is the net energy loss in this half orbit. The quantities  $t_\varepsilon$  and  $\mu$  are discussed in Section 5.

The problem of interest is the rate coefficient  $k(t)$  for an ensemble of particles whose positions evolve as realizations of  $q(t)$ . The coefficient  $k(t)$  measures the mean rate of passage of the ensemble across  $q = 0$  from one well to the other. This crossing rate and, in particular, its asymptotic value  $k \equiv k(\infty)$ , is associated with the rate constant of the process represented by the reaction coordinate. One usually focuses on the corrections to the rate obtained from transition state theory (TST) and therefore writes

$$k(t) = \kappa(t)k^{TST} \quad (4)$$

where  $k^{TST}$  is the rate obtained from transition state theory for activated crossing, which for our problem and in our units is [2]

$$k^{TST} = \frac{\sqrt{2}}{\pi} e^{-1/4k_B T}. \quad (5)$$

The deviations from this rate constant are then contained in the transmission coefficient  $\kappa(t)$ . The construction of  $\kappa(t)$  is discussed in subsequent sections. In the remainder of this work we designate the stationary or asymptotic transmission coefficient  $\kappa(t \rightarrow \infty)$  as  $\kappa_{st}$ .

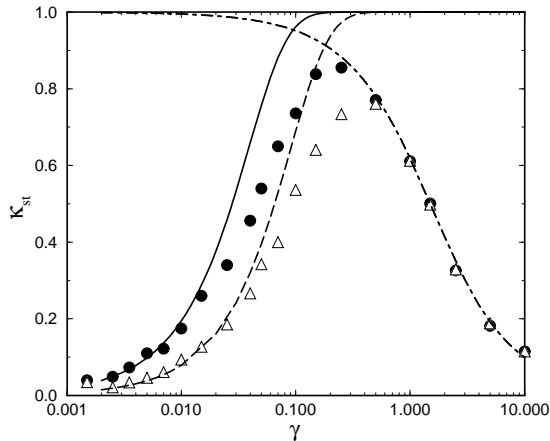


Figure 2: Transmission coefficient  $\kappa_{st}$  vs dissipation parameter  $\gamma$  for two temperatures obtained from direct simulation of Eq. (1) as described in Section 3. Solid circles:  $k_B T = 0.025$ ; triangles:  $k_B T = 0.05$ . As already predicted by Kramers, the high friction result (short-dashed curve) is independent of temperature and equal to  $-(\gamma/2) + ((\gamma^2/4) + 1)^{1/2}$ , which approaches  $\gamma^{-1}$  as  $\gamma \rightarrow \infty$ . At very low friction Kramers predicted that  $\kappa_{st}$  is proportional to  $\gamma/k_B T$ . The dashed and solid curves, based on our predictions for the behavior of  $\kappa_{st}$  beyond the very earliest linear regime, are discussed in Section 7.

The input parameters of the problem are the dissipation ( $\gamma$ ) and the temperature ( $k_B T$ ). The behavior of the stationary-state transmission coefficient  $\kappa_{st}$  as a function of these parameters, particularly as a function of  $\gamma$ , was the subject of a great deal of work in the 80's. It was already realized by Kramers that the behavior of  $\kappa_{st}$  vs  $\gamma$  would exhibit a maximum (cf. Fig. 2) since at intermediate and high dissipation (“diffusion limited regime”) the rate constant decreases with increasing dissipation while at low dissipation (“energy-diffusion limited regime”) it increases with increasing dissipation. Indeed, Kramers found that at as  $\gamma \rightarrow \infty$ ,  $\kappa_{st} \approx 1/\gamma$  while as  $\gamma \rightarrow 0$ ,  $\kappa_{st} \sim \gamma/k_B T$ . These limits were obtained from separate arguments, however, which therefore gave no indication of where precisely the “turnover” (maximum) might occur. Subsequent work attempted to address this problem [2]. The other parameter dependence, namely, on temperature, has also been the object of study. For ex-

ample, it is understood that the high-dissipation  $\kappa_{st}$  is independent of temperature whereas  $\kappa_{st}$  does depend on temperature in the low-dissipation regime. This is clearly seen in the simulation results in Fig. 2. Discussion of Fig. 2 will be resumed later.

The analysis of KT has carried the problem further in that they actually dealt with the full time-dependent evolution of the transmission coefficient. They derived an expression for  $\kappa(t)$  in terms of the time-dependent phase space density, assumed a particular form for this density, and studied how  $\kappa(t)$  goes to its steady state value as the phase space density relaxes to equilibrium. In carrying out this program, however, they relied on approximations that are appropriate for the diffusion limited regime and therefore were able to calculate  $\kappa(t)$  only in this regime. They did not check their time-dependent results against simulations, although they did confirm numerically that the (temperature-independent) steady state values for the transmission coefficient that they predict in this regime are satisfactory. They also did not deal with the energy-diffusion limited regime.

Thus, to complement the work of KT in the Markovian regime we accomplish three goals in this paper:

1. We carry out simulations of the time-dependent transmission coefficient to assess and confirm the validity of the KT formulation in the diffusion-limited regime. Their results agree very well with simulations in this regime.
2. We formulate the complementary theory for the time-dependent transmission coefficient in the energy-diffusion limited regime and compare our results with numerical simulations in this regime. Our theory captures the complex oscillatory and stationary state behavior of  $\kappa(t)$  in this regime very well.
3. We calculate and check via our simulation results the temperature dependence of the asymptotic transmission coefficient in the energy-limited diffusion regime beyond the Kramers result.

In Section 2 we briefly review the reactive flux formalism. Section 3 contains a short description of the numerical methods used in our simulations. The results of KT in the diffusion-limited regime are recalled and compared to our simulation results in Section 4.

The departure of the KT results from the simulations at low dissipation are illustrated in this section. In Sections 5 and 6 we present our theory for the time-dependent transmission coefficient  $\kappa(t)$  and its asymptotic value in the energy-diffusion limited regime. The comparison of our results with those of numerical simulations is presented in Section 7. We conclude in Section 8.

## 2 Reactive Flux Formalism

Two decades ago saw the development of the reactive flux formalism for the rate constant over a barrier [2, 7, 8]. This formalism was important because it made possible efficient numerical simulations of the rate constant without having to wait the inordinately long time that it takes a particle at the bottom of one well to climb up to the top of the barrier. In the reactive flux method the problem is formulated in terms of the particles of the thermal distribution that are sufficiently energetic to be above the barrier at the outset. In this way, it is not necessary to wait for low-energy particles (the vast majority of all the particles) to first acquire sufficiently high energies via thermal fluctuations.

We follow the notation of KT. The rate constant  $k(t)$  in the reactive flux formalism is

$$\begin{aligned} k(t) &= \frac{\langle \dot{\theta}_P(q_0) \theta_P[q(q_0, v_0, t)] \rangle}{\langle \theta_R(q_0) \rangle} \\ &= \frac{\langle v_0 \delta(q_0) \theta_P[q(q_0, v_0, t)] \rangle}{\langle \theta_R(q_0) \rangle}, \end{aligned} \tag{6}$$

where the top of the barrier is at position  $q_0 = 0$ ,  $\theta_R(x) = 1$  if  $x < 0$  and 0 otherwise, and  $\theta_P = 1 - \theta_R$ . The brackets  $\langle \rangle$  represents an average over initial equilibrium conditions. With the particular choices made in Eq. (6) one is calculating the transition rate *from* the left well *to* the right. KT proceed through a series of steps that finally yield for the transmission coefficient introduced in Eq. (4) the relation

$$\kappa(t) = \frac{m}{k_B T} \int_{-\infty}^{\infty} dv_0 v_0 e^{-mv_0^2/2k_B T} \chi(v_0, t) \tag{7}$$

where

$$\chi(v_0, t) = \int_0^\infty dq \int_{-\infty}^\infty dv W(q, v, t; q_0 = 0, v_0) \quad (8)$$

and  $W(q, v, t; q_0 = 0, v_0)$  is the conditional phase space distribution function that corresponds to an ensemble of particles starting at  $(q_0 = 0, v_0)$  at  $t = 0$ .

The (nonequilibrium) conditional probability distribution  $W$  clearly lies at the crux of the calculation: it is the distribution associated with a Langevin equation or a generalized Langevin equation that describes the evolution of the position  $q(t)$  and momentum  $p(t) = mv(t)$  of the ensemble of particles. In the problem of interest here,  $W$  is the distribution associated with Eq. (1), that is, it is the solution of the Fokker-Planck equation (we set the mass equal to unity)

$$\frac{\partial W}{\partial t} = -\frac{\partial}{\partial q}(pW) + \frac{\partial}{\partial p} \left[ \left( \gamma p + \frac{dV(q)}{dq} \right) W \right] + \gamma k_B T \frac{\partial^2 W}{\partial p^2}. \quad (9)$$

with appropriate initial and boundary conditions.

### 3 Simulations

The numerical solution of Eqs. (1) is performed according to the following main steps. The integration is carried out using the second order Heun's algorithm [9], which has been tested in different stochastic problems with very reliable results [10]. A very small time step is used, ranging from 0.001 to 0.0001, as in Ref. [7]. The numerical evaluation of the transmission coefficient  $\kappa(t)$  follows the description of Refs. [7, 8]. We start the simulation with  $N$  particles (either 4000 or 1000 depending of the circumstances), all of them above the barrier at  $q = 0$ , half with a positive velocity distributed according to the Boltzmann distribution in energy, which translates to the velocity distribution  $v \exp(-v^2/2k_B T)$ , and the other half with the same distribution but with negative velocities.

The transmission coefficient is extracted from these sets of simulated data by calculating



[7]

$$\kappa(t) = \frac{N_+(t)}{N_+(0)} - \frac{N_-(t)}{N_-(0)}, \quad (10)$$

where  $N_+(t)$  and  $N_-(t)$  are the particles that started with positive velocities and negative velocities respectively and at time  $t$  are in or over the right hand well (i.e. the particles for which  $q(t) > 0$ ).

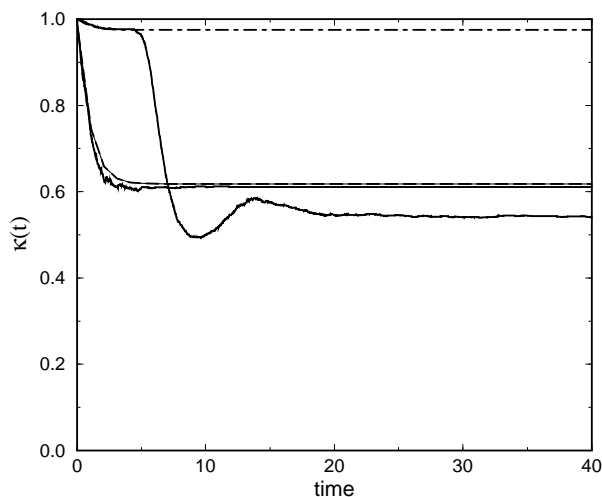


Figure 3: Transmission coefficient  $\kappa(t)$  vs time for two values of the dissipation parameter  $\gamma$  and for temperature  $k_B T = 0.025$ . The solid curves are the results of our numerical simulations. For high dissipation ( $\gamma = 1.0$ , on the right of the maximum in Fig. 2), the transmission coefficient decreases monotonically. For low dissipation ( $\gamma = 0.05$ , on the left of the maximum in Fig. 2) the decay is oscillatory. The dashed curves are those calculated from the theory of KT (cf. Eq. (12)), which is seen to predict the numerical results very well for high dissipation, the regime for which the theory is designed. The agreement seen in the figure is typical for large dissipation parameters. Not surprisingly, the theory fails at low dissipation.

Figure 3 exhibits examples of the temporal behavior of the transmission coefficient, Eq. (10), for two typical different parameter regimes as described in the figure caption. Of interest in this paper is the low-dissipation oscillatory behavior, which is illustrated and discussed further in subsequent sections.

As discussed by Straub et al. [8], whereas the exact transmission coefficient reaches a

constant non-zero value that corresponds to the equilibrium transition rate for the problem, the transmission coefficient calculated using the reactive flux method flattens out but continues to decrease with time. If the temperature is low, this decrease is slow and the results appear flat on the sort of time scale shown in Fig. 2. In this case the value of  $\kappa(t)$  in this flat region is identified with  $\kappa_{st}$ . If the temperature is not so low, then the decaying tail is extrapolated back to its intersection with the vertical axis according to the relation

$$\kappa(t) \sim \kappa_{st} e^{-Kt} \quad (11)$$

where  $K$  is the decay constant of the tail. Thus, the value of the intersection is identified as  $\kappa_{st}$ .

The numerical values of  $\kappa_{st}$  presented in Fig. 2 are obtained according to these schemes. Numerical uncertainties are fairly large and difficult to avoid for small values of  $\kappa_{st}$ .

## 4 Diffusion Limited Regime

Equation (9) can not be solved exactly for the bistable potential, and therefore the distribution  $W$  is the quantity in the calculation of the transmission coefficient that requires approximation. The quality of the result of course depends on the quality of the approximations. KT focus on the regime of moderate to high dissipation, that is, on the Grote-Hynes model. In this regime it is appropriate to adapt the theory of Adelman [11] to the assumption that the barrier is parabolic. With this approximation for the conditional probability, KT derive expressions for  $\kappa(t)$  from which the Grote-Hynes results are recovered in the long-time limit. Their result is

$$\kappa(t) = \frac{e^{\mu_1 t} - e^{\mu_2 t}}{\left( e^{2\mu_1 t} \frac{\omega^2}{\mu_1^2} + e^{2\mu_2 t} \frac{\mu_1^2}{\omega^2} + 2e^{-\gamma t} - 4 \frac{\omega_1^2}{\omega^2} \right)^{1/2}} \quad (12)$$

where

$$\omega_1 \equiv \sqrt{\frac{\gamma^2}{4} + \omega^2}, \quad \mu_{1,2} = -\frac{\gamma}{2} \pm \omega_1, \quad (13)$$

and  $\omega$  is the “frequency” of the top of the barrier, which for the potential (3) is unity.

In order to assess the KT results and their regime of validity, we point again to Fig. 2, where we show the asymptotic transmission coefficient as a function of the dissipation parameter obtained from simulations based on Eq. (7). In this figure we have exhibited the results for two temperatures. The high dissipation side of the curve is independent of temperature, but the low dissipation transmission coefficient is inversely proportional to temperature. The short-dashed curve is the Kramers/Grote-Hynes result (and therefore also the result recovered by KT). Clearly, it is excellent at high dissipation (a well-known result), but does not capture the turnover and subsequent decrease in the transmission coefficient as one enters the energy-diffusion limited regime.

Figure 3 exhibits a typical simulation result in the high dissipation regime ( $\gamma = 1.0$ ) (monotonic somewhat jagged curve) and also the associated KT prediction Eq. (12) (dashed curve). The agreement is seen to be very good over the full time-dependence of the transmission coefficient. The very small discrepancy in the asymptotic regime is also typical, with the theoretical results slightly above those of the simulation. This may in part be due to the issues surrounding Eq. (11). In any case, this degree of agreement between the KT theory and the simulations is typical in the regime well beyond the turnover in Fig. 2. The theory fails, however, at low dissipation parameters. In Fig. 3 we show typical results in this regime – these are for  $\gamma = 0.05$  and  $k_B T = 0.025$ . Although the two values of  $\gamma$  that we have chosen for this figure lead to similar values of the stationary transmission coefficient, the decay towards these values is clearly very different in the two cases. The simulation results (continuous curve) and the KT result (dotted curve) agree at early times, until the simulation results rather suddenly drop and settle in an oscillatory way to a completely different lower asymptotic value than the theoretical result [12]. The KT result in fact asymptotes to the Grote-Hynes rate, which in this regime is not correct. In the next sections we obtain results that predict the correct oscillatory and asymptotic behavior of the transmission coefficient in the very low dissipation regime.

## 5 Energy-Diffusion Limited Regime - Orbits

In this section and the next, we detail the approach complementary to that of KT to obtain analytic results for the time-dependent transmission coefficient in the energy-diffusion limited regime. Our results are compared to numerical simulations in Section 7.

For our calculation it is convenient to write the transmission coefficient as (cf. Eq. (10))

$$\kappa(t) = \kappa_+(t) - \kappa_-(t), \quad (14)$$

where  $\kappa_+(t)$  is the fraction of particles that started above the barrier with positive velocity  $v_0 > 0$  whose coordinate  $q(t) > 0$ , i.e., those that are over or in the right hand well at time  $t$  given that they were over the right hand well initially, and  $\kappa_-(t)$  the fraction that started above the barrier with negative velocity  $v_0 < 0$  and are over or in the right hand well at time  $t$ .

When dissipation is very slow, the particles that start above the barrier lose their energy very slowly as they orbit around at an almost constant energy during each orbit (recrossing the barrier many times if they start with sufficiently high energy). One can calculate the approximate energy loss per orbit and thus keep track of how long it takes a particle of a given initial energy above the barrier to lose enough energy to be caught in one well or the other. There is of course a thermal distribution of such particles above the barrier, and the time that it takes the ensemble to lose enough energy to be caught in a well is correspondingly distributed.

The principal ingredients in this calculation are thus

1. The time that it takes to complete an orbit;
2. The energy loss per orbit;
3. The distribution of times at which particles eventually become trapped in one well or the other.

In this section we concentrate on the first two of these ingredients. The third component, which then leads directly to the transmission coefficient, is considered in the next section.

Because of the slow energy variation it is here convenient to rewrite the dynamical equations (1) in terms of the displacement and the *energy*

$$E = \frac{p^2}{2} + V(q) \quad (15)$$

instead of the momentum [13, 14]. This simple change of variables leads to

$$\dot{q} = \{2[E - V(q)]\}^{1/2} \quad (16)$$

$$\dot{E} = -2\gamma[E - V(q)] + f(t) \{2[E - V(q)]\}^{1/2}. \quad (17)$$

This set can of course not be solved exactly either, but one can take advantage of the fact that for small dissipation  $\gamma$  the temporal variation of the energy is much slower than that of the displacement.

The first quantity to calculate (approximately) is the time that it takes a particle of energy  $E$  above the barrier ( $E > 1/4$ ) to complete one passage from  $q = 0$  to the edge  $q_+$  of the potential well and back to  $q = 0$  (cf. Fig. 1). For this calculation we assume (this is the approximation) that the energy  $E$  remains fixed during this passage.  $q_+$  is given by the solution of  $E = V(q)$ , i.e., by  $q_+ = (1 + \sqrt{4E})^{1/2}$ . We label  $t(E)$  this time of travel between  $q = 0$  and  $q = q_+$  and back to  $q = 0$  and call this a “half-orbit.” The time  $t(E)$  is then simply obtained by integrating Eq. (16):

$$t(E) = 2 \int_0^{q_+} \frac{dq}{\{2[E - V(q)]\}^{1/2}}. \quad (18)$$

With the potential (3) this can be expressed in terms of a complete elliptic integral of the first kind,  $\mathcal{K}(z)$ :

$$t(E) = \frac{2}{(4E)^{1/4}} \mathcal{K} \left( \frac{1 + 2\sqrt{E}}{4\sqrt{E}} \right). \quad (19)$$

For low temperatures the particles that determine the behavior of the transmission coefficient are primarily those just above the top of the barrier. For these energies an excellent approx-

imation to Eq. (19) shows that the time to traverse the potential depends logarithmically on the excess energy of the particle above the barrier:

$$t(E) \approx \ln \frac{16}{(E - \frac{1}{4})}. \quad (20)$$

It is convenient for this and subsequent results to introduce the notation

$$\varepsilon \equiv E - 1/4, \quad (21)$$

that is, the energy *above* the barrier. In terms of this energy

$$t_\varepsilon \equiv t(E) \approx \ln \frac{16}{\varepsilon} \quad (22)$$

(cf. Fig. 1). The corrections to Eq. (22) are of  $O(\varepsilon \ln \varepsilon)$ .

*Equation (22) is one of the essential results of this section.*

The energy of the particle of course does not in fact remain constant as the particle orbits around. Kramers calculated this energy loss in his theory of energy-diffusion limited reactions in terms of the action of the particle. We recover his result using the following physically transparent argument. To estimate the actual energy loss, say, along a half orbit, in the simplest approximation one neglects the fluctuations in Eq. (17) (since particles at the high end of the energy distribution primarily lose energy - this overestimates the energy loss) and integrates over a time interval  $t(E)$ . Note that ignoring the fluctuations is *not* tantamount to “ignoring the thermal effects,” since the principal thermal effects lie in the initial distribution of energies, which we take into account exactly. Subsequently we also take account of the fluctuations ignored in this simplest approximation. The  $q(t)$  dependence in Eq. (17) still poses a problem, though, because it is in general an incomplete elliptic integral itself amenable only to numerical integration. However, since  $q$  changes rapidly compared to  $E$ , it would appear reasonable to perform an average of the  $q$ -dependent term over a passage from  $q = 0$  to  $q_+$ . This leads to the approximation

$$\dot{E} = -2\gamma F(E) \quad (23)$$

where

$$F(E) \equiv \int_0^{q+} dq P_E(q) [E - V(q)] \quad (24)$$

and  $P_E(q)$  is the probability density that  $q(t) = q$ . The assumption that this probability density is in turn proportional to the inverse of the velocity at  $q(t)$ , i.e.,  $P_E(q) \propto 1/\dot{q}$  [13, 14], leads with Eq. (16) and appropriate normalization to

$$P_E(q) = \frac{\sqrt{2}}{t(E)} \frac{1}{[E - V(q)]^{1/2}}. \quad (25)$$

The integral in Eq. (24) can then be expressed in terms of complete elliptic integrals. For the energies of interest here an excellent approximation is obtained by retaining the  $E$ -dependent contribution  $t(E)$  in Eq. (25) (which is singular as  $E \rightarrow 1/4$ ) but to set  $E = 1/4$ , the barrier height, elsewhere in the integrand. We thus obtain

$$F(E) \approx \frac{2}{3} \ln \frac{16}{(E - \frac{1}{4})} \approx \frac{2}{3t(E)}, \quad (26)$$

Thus, for a first estimate of the energy loss per half orbit one might use Eq. (23) with (26):

$$\dot{E} = -\frac{4\gamma}{3} \frac{1}{t(E)} \quad (27)$$

The next question then is: on the basis of the approximate equation (27), how much energy does a particle that begins with energy  $E$  actually lose per half orbit? The answer of course depends on the energy – in particular, according to Eq. (27), it depends on the time that it takes that particle to complete its half orbit. Let  $\mu(E)$  be the energy loss in a half orbit of a particle that has initial energy  $E$ . The deterministic equation Eq. (27) can be integrated directly and to give in terms of the energy  $\varepsilon$  above the barrier

$$\left( \frac{4\gamma}{3} - \mu \right) \ln \frac{16}{\varepsilon} = (\varepsilon - \mu) \ln \frac{\varepsilon - \mu}{\varepsilon} + \mu. \quad (28)$$

The solution  $\mu(\varepsilon)$  of this equation clearly depends on the initial energy  $\varepsilon$  of the particle

above the barrier. It is in fact not difficult to see that  $\mu(\varepsilon)$  increases with  $\varepsilon$ . However, this dependence is sufficiently mild that the error made in ignoring this variation is no larger than the effect of the corrections of  $O(\varepsilon \ln \varepsilon)$  that have been ignored in Eq. (22). We can therefore pick a convenient energy above the barrier to calculate this loss in a half orbit. An upper bound to the solution is obtained by setting  $\varepsilon \gg \mu$  in Eq. (28), which immediately yields the simple relation between the energy loss per half orbit and the dissipation parameter

$$\mu = \frac{4}{3}\gamma. \quad (29)$$

This result agrees with that obtained via weak-collision arguments or small dissipation arguments by a variety of essentially equivalent routes. At the other extreme, we can set  $\varepsilon = \mu$ . Particles with this energy have just enough energy to complete a half orbit from  $q = 0$  to  $q_+$  and back to the origin. Solution of Eq. (28) in this case leads to a  $\mu$  that is somewhat smaller than Eq. (29), by approximately 10-15% for dissipation parameters in the energy-diffusion limited regime.

We shall call the value Eq. (22) of  $\mu$  the “bare” energy loss per half orbit and keep in mind that it is an upper bound for  $\mu$ .

*Equation (29) is the second important result of this section.*

In the absence of fluctuations, the only approximations (to order  $\varepsilon \ln \varepsilon$ ) have been to average over a half orbit in calculating the time for the return of a particle to the origin, and to assume that in the calculation of this period the energy loss of the particle over the half orbit is negligible. Thus, we have approximated the evolution of the energy of a particle as determined by Eqs. (16) and (17) with  $f(t) = 0$  by simply assuming an energy loss of  $\mu$  at the end of each half orbit. In Fig. 4 we show the results of the exact integration of Eqs. (16) and (17) in the absence of fluctuations for a particle starting at  $q = 0$  with an energy  $\varepsilon = 0.04$  above the barrier and moving toward the right. The bottom panel shows the trajectory of the particle,  $q(t)$ . The particle orbits back and forth above the barrier several times before getting trapped in the left well. The top panel shows the associated phase space portrait. The middle panel shows the decay of the energy (solid curve). The decay is not entirely uniform because the rate of energy loss when the particle has high



kinetic energy (i.e. as it goes over the deepest portions of the wells) is greater than when its kinetic energy is low. However, this non-uniformity is very mild. Our approximation is given by the circular symbols: we assume an energy loss of  $\mu$  per half orbit, and the symbols are placed at the times of completion of each half orbit as predicted by our theory. Once the particle gets trapped, its orbits become smaller and the energy loss per orbit smaller, but these dynamics are in any case not relevant to our problem. We conclude that in the absence of fluctuations the assumption of an equal loss of energy  $\mu$  in the course of each half orbit during the recrossing process is appropriate. The other theoretical information used in drawing the symbols in the middle panel of the figure are the times it takes to complete each of the half orbits. The lower panel in Fig. 4 shows crossings at the times given in the second column of Table 1. Those predicted by Eq. (22) are presented in the fourth column. To obtain these numbers we subtract an energy  $\mu = 4\gamma/3$  after each half orbit and calculate the appropriate  $t_\varepsilon$  for the next half orbit. The agreement is clearly quite good.

Consider now the evolution of particles in the presence of thermal effects. In Fig. 5 we again show the results of the exact integration of Eqs. (16) and (17), but now in the presence of fluctuations corresponding to a temperature  $k_B T = 0.025$ . The second and third panels represent ensemble averages over 500 particles all starting at  $q = 0$  and moving toward the right with an initial energy  $\varepsilon = 0.04$  above the barrier. The ensemble average is over different realizations of the fluctuations. The bottom panel shows the average trajectory of the particles,  $\langle q(t) \rangle$ . On average, the particles orbit back and forth above the barrier several times. About half of the particles eventually get trapped in the left well and the other half in the right, whence the average trajectory settles down to values near zero. The top panel shows the associated phase space portrait for a typical particle of the ensemble. The middle panel shows the decay of the average energy (solid curve). The decay is a bit noisier than that of the deterministic case of Fig. 4 because the stochastic ensemble is not very large (the fluctuations are of order  $O(N^{-1/2})$  where  $N$  is the number of particles). Our approximation (which neglects thermal effects) is again given by the circular symbols: we have again assumed an energy loss of  $\mu$  per half orbit, and the symbols are placed at the times of completion of each half orbit as predicted by our theory. Again, the agreement is excellent. We conclude that on these time scales even in the presence of fluctuations the

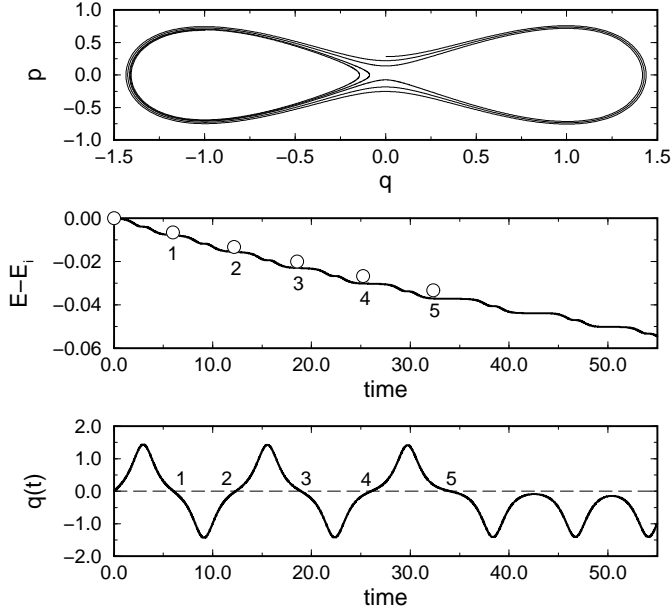


Figure 4: Simulation of the evolution of a single particle according to Eqs. (16) and (17) with no fluctuations. The particle starts at  $q = 0$  moving toward the right and with initial energy  $E_i = 0.254$  ( $\varepsilon_i = 0.04$ ). The dissipation parameter is  $\gamma = 0.005$ . Top panel: phase space portrait. Middle panel: the decay of the energy (solid curve). Bottom panel: the particle trajectory. The times at which the particle crosses  $q = 0$  have been labeled consecutively – in this case there are five such times before the particle becomes trapped. Circular symbols: the decay of the energy according to our approximation. The symbols are placed at the theoretical barrier recrossing times.

assumption of an equal loss of energy  $\mu$  in the course of each half orbit during the recrossing process is appropriate, and that this value of  $\mu$  is essentially that obtained disregarding the fluctuations. Again, the other theoretical information used in drawing the symbols in the figure are the times it takes to complete each of the half orbits. The crossings observed in the lower panel in Fig. 5 occur at the times shown in the third column of Table 1. Note that the crossing times are now just a little shorter than in the deterministic simulation, an indication that the particles have a bit more energy as they orbit and are thus moving a bit faster. This in turn indicates that the energy loss per orbit here is actually a bit smaller than in the deterministic case (just barely perceptibly so on the energy scale of the middle panels in the figures). We interpret this as the effect of thermal fluctuations that counteract the energy loss. On these short time scales the thermal fluctuations barely begin

to have an effect on the evolving particles, and hence their behavior is very well captured by the dissipative component. We will see subsequently that although the short time behavior (such as shown in these figures) is well captured by an energy loss rate that is independent of the fluctuations, at longer times the fluctuations play a more important role and the corresponding  $\mu$  should be appropriately renormalized.

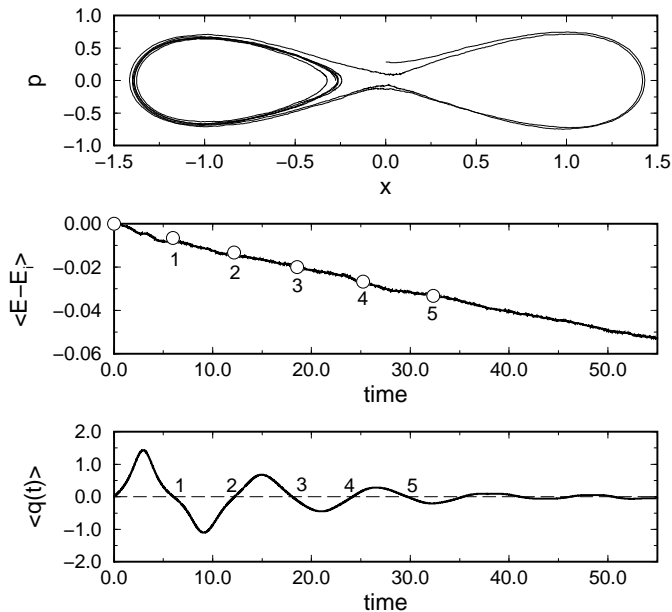


Figure 5: Simulation of the evolution of 500 particles according to Eqs. (16) and (17) with fluctuations corresponding to a temperature  $k_B T = 0.025$ . The initial energy of each particle above the barrier is  $\varepsilon_i = 0.04$ , and the dissipation parameter is  $\gamma = 0.005$ . Top panel: phase space portrait of a typical particle. Middle panel: the decay of the average energy (solid curve). Bottom panel: the average particle trajectory. The times at which the particles on average cross  $q = 0$  have been labeled consecutively – in this case there are five such times before the particle becomes trapped. Circular symbols: the decay of the energy according to our approximation. The symbols are placed at the theoretical barrier recrossing times.

To estimate the correction to Eq. (29) due to the thermal fluctuations we return to the full set Eqs. (16) and (17) and consider the Fokker-Planck equation associated with this set

for the probability density  $W(q, E, t|q_0 = 0, E_0)$ :

$$\begin{aligned} \frac{\partial}{\partial t} W = & -\frac{\partial}{\partial q} \{2[E - V(q)]\}^{1/2} W + 2\gamma \frac{\partial}{\partial E} [E - V(q)] W \\ & + \gamma k_B T \frac{\partial}{\partial E} \{2[E - V(q)]\}^{1/2} \frac{\partial}{\partial E} \{2[E - V(q)]\}^{1/2} W. \end{aligned} \quad (30)$$

To find an equation for the evolution of the average energy  $\langle E(t) \rangle$  we multiply Eq. (30) by  $E$  on the left and integrate over  $q$  and  $E$ . Upon integration by parts all boundary terms vanish and one is left with

$$\frac{d}{dt} \langle E \rangle = -2\gamma \langle E - V(q) \rangle + \gamma k_B T \quad (31)$$

where

$$\langle f(q, E) \rangle \equiv \int_0^\infty dE \int dq W(q, E, t|q_0 = 0, E_0) f(q, E) \quad (32)$$

and the integral over  $q$  is over the region where  $V(q) < E$ . A well-known generalization of the argument surrounding Eq. (25) in the energy-diffusion limited regime is to assume that the probability density can be separated in the form [13, 14]

$$W(q, E, t|q_0 = 0, E_0) \approx w(E, t|E_0) P_E(q) \quad (33)$$

(the steps to obtain Eq. (28) are consistent with this assumption in the special case that  $w$  evolves deterministically). The average of Eq. (31) with respect to  $q$  is then equivalent to the earlier average over a half-orbit at fixed  $E$ . With the assumption that we can replace  $\langle t(E)^{-1} \rangle$  with  $t(\langle E \rangle)^{-1}$  this finally leaves us with the evolution equation for the mean energy that modifies (27) in that it takes thermal fluctuations into account:

$$\langle \dot{E} \rangle = -\frac{4\gamma}{3} \frac{1}{t(\langle E \rangle)} + \gamma k_B T. \quad (34)$$

The solution of this equation again clearly depends on the initial energy of the particle,

	Simulation	Simulation	Theory
	Deterministic	$k_B T = 0.025$	
$t_0$	0.00	0.00	0.00
$t_1$	6.03	6.04	5.99
$t_2$	12.32	12.20	12.16
$t_3$	18.94	18.06	18.56
$t_4$	26.03	24.15	25.24
$t_5$	34.04	29.70	32.33

Table 1: Zero crossing times of the orbits shown in Figs. 4 and 5. Second column: simulation results of Fig. 4. Third column: simulation results of Fig. 5. Fourth column: theoretical results.

and the arguments surrounding the choice (29) still apply. An exact explicit solution of Eq. (34) (even to the orders of approximation considered here) is not possible, but a rough approximation for low temperatures is

$$\mu(T) = \frac{4}{3}\gamma - \gamma k_B T \ln \frac{12}{\gamma}. \quad (35)$$

Of course, numerical integration of Eq. (34) is trivial, and in our further analysis we use the outcome of such integration. For example, for  $\gamma = 0.005$ , a value used in a number of our simulations, Eq. (34) leads to  $\mu(T) = 0.004907$  for  $k_B T = 0.025$  and to  $\mu(T) = 0.004485$  for  $k_B T = 0.035$ . These are to be compared with the estimate in Eq. (29), which is  $\mu = 0.006667$ . Although at short times we have seen that the “bare” value of  $\mu$  yields excellent agreement with simulations, these “renormalized” values do play a more important role at long times, as will be seen in the next section.

*The expression (35) or, more precisely, the result of integrating Eq. (34), is the third essential result of this section.*

## 6 Energy-Diffusion Limited Regime - Transmission Coefficient

The calculation of the time-dependent transmission coefficient, the goal of this work, is based on the principal results of the previous section, namely, the time  $t(E) \equiv t_\varepsilon$  it takes a particle of energy  $\varepsilon$  above the barrier to complete a half orbit, and the energy loss  $\mu$  in the course of this time. In order to carry out this calculation, we must keep track of where the particles that start above the barrier are at any time before they get trapped in one or the other of the wells, and at what time each particle becomes trapped in one well. These quantities of course depend on the initial energy of the particle, which is in turn distributed thermally.

The accounting that leads to the result for the transmission coefficient  $\kappa(t)$  turns out to be more transparent if we note that due to the symmetry of the problem the following interpretation of the terms in Eq. (14) leads precisely to the same result as the description presented there. We can imagine that *all* particles are forced to start with a positive velocity  $v_0 > 0$ . Then  $\kappa_+(t)$  is, as before, the fraction of particles that at time  $t$  are over or in the right hand well, but now  $\kappa_-(t)$  can be interpreted as the fraction of particles that at time  $t$  are over or in the left hand well. Furthermore, with this interpretation it is clear that

$$\kappa_-(t) = 1 - \kappa_+(t) \tag{36}$$

so it is sufficient to follow one or the other.

With this interpretation we thus imagine that all particles above the barrier start at  $q_0 = 0$  and with a positive velocity  $v_0$  distributed according to the Boltzmann distribution. Since the energy loss per half orbit is  $\mu$  essentially independently of the energy of the particles (subject to the approximations and conditions discussed in the last section), keeping track of particles is conveniently done in “layers” of energy thickness  $\mu$ . Although the energy loss per half orbit is essentially independent of energy, the time for a half orbit is not, since particles of higher energy return to  $q = 0$  faster than those of lower energy. This time dispersion must be accounted for carefully in constructing  $\kappa(t)$ .

Initially the particles are distributed according to a Boltzmann distribution at tempera-

ture  $T$ . The fraction of particles that are above the barrier is

$$P(E > 1/4) = \frac{1}{k_B T} \int_{1/4}^{\infty} e^{-E/k_B T} = e^{-1/4 k_B T}. \quad (37)$$

We are interested in keeping track of only this fraction and, in particular, of the fraction of this fraction that is over one well or the other as time proceeds. Therefore, we normalize this initial fraction to unity, i.e., the distribution of interest is

$$p(\varepsilon) = \frac{1}{k_B T} e^{-\varepsilon/k_B T}, \quad 0 < \varepsilon < \infty. \quad (38)$$

Initially all particles are over the right hand well, i.e.,

$$\kappa_+(0) = \int_0^{\infty} d\varepsilon p(\varepsilon) = 1, \quad \kappa_-(0) = 0 \quad (39)$$

and therefore

$$\kappa(0) = 1. \quad (40)$$

All those particles that start with an energy between 0 and  $\mu$  above the barrier never leave the right hand well since by the time they return to  $q = 0$  they will have lost energy  $\mu$  and will thus be below the top of the barrier and unable to move out of the well. The remainder, those of energy greater than  $\mu$  above the barrier,  $\varepsilon > \mu$ , do come back and recross the barrier to the other side. However, they do so at different times depending on their energy. We can write this as follows:

$$\kappa_+(t) = 1 - \frac{1}{k_B T} \int_{\mu}^{\infty} d\varepsilon e^{-\varepsilon/k_B T} \theta(t - t_{\varepsilon}) + \dots, \quad (41)$$

where the Heaviside theta function  $\theta(x) = 1$  for  $x > 0$  and  $= 0$  for  $x < 0$ . The theta function insures that recrossing occurs at the right time for that energy and no sooner. The  $\dots$  indicate that the calculation is not yet complete, since we need to continue to keep track of particles that recross back from the left well to the right, and so on. The theta function in

Eq. (41) can be implemented by adjusting the limits of integration:

$$\begin{aligned}\kappa_+(t) &= 1 - \frac{1}{k_B T} \int_{f_1(t)}^{16} d\varepsilon e^{-\varepsilon/k_B T} + \dots, \quad 0 < t < \ln \frac{16}{\mu}, \\ &= 1 - \frac{1}{k_B T} \int_{\mu}^{16} d\varepsilon e^{-\varepsilon/k_B T} + \dots, \quad \ln \frac{16}{\mu} < t < \dots.\end{aligned}\tag{42}$$

Here  $f_1(t)$  is the inverse of the half orbit time, that is,  $\varepsilon = f_1(t)$  is the solution of the relation

$$t = t_\varepsilon = \ln \frac{16}{\varepsilon},\tag{43}$$

which immediately leads to

$$f_1(t) = 16e^{-t}.\tag{44}$$

Note that the upper limit of the range of the time variable in the first line of Eq. (42) is precisely the time it takes a particle of energy  $\mu$  above the barrier to complete a half orbit, that is, Eq. (43) with  $\varepsilon = \mu$ . During this time all the particles with initial energies above  $\varepsilon = \mu$  will have recrossed the barrier at least once, and all the particles with energies below  $\varepsilon = \mu$  are trapped in the right hand well. The upper limits of integration are written as 16 (rather than  $\infty$ ) because our approximation for  $t_\varepsilon$  (cf. Eqs. (19) and (20)) breaks down for higher energies, but 16 is, for all practical purposes, infinite when the energy loss per orbit is of order  $\gamma$  and  $\gamma$  is very small. In our subsequent discussion of the time dependence of the transmission coefficient  $\gamma$  is of order  $10^{-2}$ . On the other hand, the time intervals that define the ranges of behavior *do* involve precisely  $\ln(16/\mu)$  because for small  $\mu$  this is the leading contribution to the elliptic integral discussed in Section 5. The integrals in Eq. (42) can be



done explicitly. Treating the upper limit as  $\infty$  we find

$$\begin{aligned}\kappa_+(t) &= 1 - e^{-f_1(t)/k_B T} + \dots, & 0 < t < \ln \frac{16}{\mu}, \\ &= 1 - e^{-\mu/k_B T} + \dots, & \ln \frac{16}{\mu} < t < \dots.\end{aligned}\quad (45)$$

As before, the  $\dots$  indicate that the calculation still continues.

The next stage of the calculation is to follow the particles that recrossed the barrier once and find themselves over the left well. Those that started at  $t = 0$  with energy in the range  $\mu < \varepsilon < 2\mu$  above the barrier and lost energy  $\mu$  in their first orbit have entered the region above the left well with energy between 0 and  $\mu$  above the barrier, and will therefore never make it out of the left well. Only those that started with energy greater than  $2\mu$  above the barrier and thus recrossed the barrier with energy greater than  $1/4 + \mu$  will be able to orbit over the left well and return to  $q = 0$  and eventually recross once again to the right hand well. The following continuation of Eq. (41) captures this behavior:

$$\kappa_+(t) = 1 - \frac{1}{k_B T} \int_{\mu}^{\infty} d\varepsilon e^{-\varepsilon/k_B T} \theta(t - t_{\varepsilon}) + \frac{1}{k_B T} \int_{2\mu}^{\infty} d\varepsilon e^{-\varepsilon/k_B T} \theta(t - t_{\varepsilon} - t_{\varepsilon-\mu}) + \dots. \quad (46)$$

Again, the theta functions insure the correct timing of the recrossings and they can be implemented by adjusting the limits of integration:

$$\begin{aligned}\kappa_+(t) &= 1 - \frac{1}{k_B T} \int_{f_1(t)}^{16} d\varepsilon e^{-\varepsilon/k_B T} + \frac{1}{k_B T} \int_{f_2(t)}^{16} d\varepsilon e^{-\varepsilon/k_B T} + \dots, & 0 < t < \ln \frac{16}{\mu}, \\ &= 1 - \frac{1}{k_B T} \int_{\mu}^{16} d\varepsilon e^{-\varepsilon/k_B T} + \frac{1}{k_B T} \int_{f_2(t)}^{16} d\varepsilon e^{-\varepsilon/k_B T} + \dots, & \ln \frac{16}{\mu} < t < 2 \ln \frac{16}{(2!)^{1/2} \mu}, \\ &= 1 - \frac{1}{k_B T} \int_{\mu}^{16} d\varepsilon e^{-\varepsilon/k_B T} + \frac{1}{k_B T} \int_{2\mu}^{16} d\varepsilon e^{-\varepsilon/k_B T} + \dots, & 2 \ln \frac{16}{(2!)^{1/2} \mu} < t < \dots.\end{aligned}\quad (47)$$

The function  $f_2(t)$  is the inverse of the sum of the two half orbit times, the first half orbit

being that over the right hand well with energy  $\varepsilon$ , and the second that over the left well with energy  $\varepsilon - \mu$ . In other words,  $\varepsilon = f_2(t)$  is the solution of the relation

$$t = t_\varepsilon + t_{\varepsilon-\mu} = \ln \frac{16}{\varepsilon} + \ln \frac{16}{\varepsilon - \mu}. \quad (48)$$

Exponentiation leads to

$$16^2 e^{-t} = \varepsilon(\varepsilon - \mu). \quad (49)$$

This is a quadratic equation that can easily be solved:

$$f_2(t) = \frac{\mu + \sqrt{\mu^2 + 1024e^{-t}}}{2}. \quad (50)$$

The upper limit of the second range of the time variable in Eq. (47) is the time it takes a particle of initial energy  $2\mu$  above the barrier to complete two half orbits, that is, Eq. (48) with  $\varepsilon = 2\mu$ . These particles are trapped in the left well during their second half orbit. The integrals can again be carried out explicitly to obtain:

$$\begin{aligned} \kappa_+(t) &= 1 - e^{-f_1(t)/k_B T} + e^{-f_2(t)/k_B T} + \dots, & 0 < t < \ln \frac{16}{\mu}, \\ &= 1 - e^{-\mu/k_B T} + e^{-f_2(t)/k_B T} + \dots, & \ln \frac{16}{\mu} < t < 2 \ln \frac{16}{(2!)^{1/2} \mu}, \\ &= 1 - e^{-\mu/k_B T} + e^{-2\mu/k_B T} + \dots, & 2 \ln \frac{16}{(2!)^{1/2} \mu} < t < \dots. \end{aligned} \quad (51)$$

The pattern for  $\kappa_+(t)$  and hence for  $\kappa(t)$  as required in Eq. (14) has thus been established. We can write the following complete result for the transmission coefficient as a function of

time:

$$\begin{aligned}
\kappa(t) &= 1 + 2 \sum_{n=1}^{\infty} (-1)^n e^{-f_n(t)/k_B T}, & 0 < t < \ln \frac{16}{\mu}, \\
&= 1 - 2e^{-\mu/k_B T} + 2 \sum_{n=2}^{\infty} (-1)^n e^{-f_n(t)/k_B T}, & \ln \frac{16}{\mu} < t < 2 \ln \frac{16}{(2!)^{1/2} \mu}, \\
&= 1 - 2e^{-\mu/k_B T} + 2e^{-2\mu/k_B T} + 2 \sum_{n=3}^{\infty} (-1)^n e^{-f_n(t)/k_B T}, & 2 \ln \frac{16}{(2!)^{1/2} \mu} < t < 3 \ln \frac{16}{(3!)^{1/3} \mu},
\end{aligned} \tag{52}$$

and so on. The function  $\varepsilon = f_m(t)$  is the solution of the relation  $t = t_\varepsilon + t_{\varepsilon-\mu} + \dots + t_{\varepsilon-(m-1)\mu}$ , which upon exponentiation turns into the  $m^{th}$  order polynomial equation (a clear generalization of the results Eq. (44) for  $m = 1$  and Eq. (49) for  $m = 2$ ):

$$(16)^m e^{-t} = \varepsilon[\varepsilon - \mu] \cdots [\varepsilon - (m-1)\mu]. \tag{53}$$

The solution of Eq. (53) can in general not be found in closed form for  $m \geq 3$ . However, an excellent approximation is

$$f_m(t) \approx [m - (m!)^{1/m}] \mu + 16e^{-t/m}. \tag{54}$$

This form is exact for  $m = 1$ , and it is exactly correct for all  $m$  at the upper limit of the time range that defines the trapping of the particles whose initial energy is  $\varepsilon = m\mu$ . In other words,  $f_m(t)$  as given in Eq. (54) is exactly correct at the particular time  $t = t_\mu + t_{2\mu} + \dots + t_{m\mu}$ .

*Equation (52) and its asymptotic limit*

$$\begin{aligned}\kappa_{st} = \kappa(t \rightarrow \infty) &= 1 + 2 \sum_{n=1}^{\infty} (-1)^n e^{-n\mu/k_B T} \\ &= \tanh\left(\frac{\mu}{2k_B T}\right).\end{aligned}\tag{55}$$

*are the principal results of this paper.* These results generalize those of KT in the Markovian regime to the energy-diffusion limited case.

It is useful to examine the information contained in the various contributions to Eq. (52) and the preceding pieces that were used to construct it. The first line contains all first recrossings of the barrier by all particles that start with sufficient energy above the barrier to recross is at least once ( $\varepsilon > \mu$ ). The function  $f_1(t)$  accounts for the fact that this first recrossing occurs at different times for particles of different initial energy, the last ones (those closest to the barrier that do make it around) recrossing at time  $t = \ln(16/\mu)$ . The particles of higher energy recross first because they are orbiting at higher velocity, and may be back for their second recrossing while those of lower energy are still awaiting their first crossing. The time distribution of the second recrossing is contained in  $f_2(t)$ . Even while this is occurring, some particles might already be undergoing their third recrossing, as contained in  $f_3(t)$ . There are fewer and fewer of these faster particles because of their initial thermal distribution – this information, too, is contained in the exponential factors. Of course while all these recrossings are going on, the particles are losing energy and, depending on their initial energy and how often they have gone around, they become trapped at sequential times as expressed in the subsequent lines of Eq. (52).

We note the nonlinear dependence of  $\kappa_{st}$  on the energy loss parameter  $\mu$  and hence on the dissipation parameter  $\gamma$ . The Kramers and other weak collision results in the energy-diffusion limited regime correspond to the retention of only the leading term in a small- $\gamma$  expansion of our result, which then yields  $\kappa_{st} \sim \gamma/k_B T$ .

The detailed behavior of the time-dependent transmission coefficient as given by Eq. (52), and its asymptotic value Eq. (55), are compared with simulations in the next section.

## 7 Discussion of Results and Comparisons with Numerical Simulations

Figures 6 and 7 show the transmission coefficient  $\kappa(t)$  as a function of time for two sets of parameters. In Fig. 6 the dissipation parameter is  $\gamma = 0.005$  and the temperature is  $k_B T = 0.025$ ; in Fig. 7 they are  $\gamma = 0.01$  and  $k_B T = 0.05$ . Note that these are the only input parameters. The solid curves are simulations of an ensemble of 4000 particles. Each particle follows the equations of motion (1), and the transmission coefficient is calculated from the resulting trajectories according to the reactive flux formalism described earlier. The distinctive features of the time dependence are 1) the time at which the transmission coefficient drops rather abruptly from its initial value of unity, and the slope of this drop; 2) the frequencies and amplitudes of the oscillations; and 3) the asymptotic value, identified as the equilibrium value  $\kappa_{st}$  of the transmission coefficient. The dashed curves are the result of our theory, Eq. (52), with the bare value  $\mu = 4\gamma/3$  for the energy loss per half orbit. We stress that there are no adjustable parameters in these curves. The agreement between the theory and simulations is clearly very good in both cases. Without adjustable parameters, the theory captures each of the three distinctive features listed above. Indeed, we stress that with a single expression we are able to reproduce the temporal behavior of the system over essentially *all* time scales.

First we discuss those aspects of the theory that work extremely well, and then we suggest ways in which improvements could be made if even closer agreement is desired. The theory essentially *exactly* captures the first striking feature in the transmission coefficient, namely, the time and slope of the first abrupt drop. The drop corresponds precisely to the point at which the KT theory and therefore also the Grote-Hynes theory deviate from the simulation results in Fig. (3) (the parameter values there and here are different). The time of the drop and the slope of the first drop are determined by the particles that first recross from one well to the other. Although this time behavior is contained in the full sum of the first line of Eq. (52), the first portion of the sum, that is, the terms shown explicitly in Eq. (45), already capture this behavior very well. These terms account for the first crossing over the barrier and do not include the effects of recrossings (which are contained in the higher  $f_m(t)$ , as

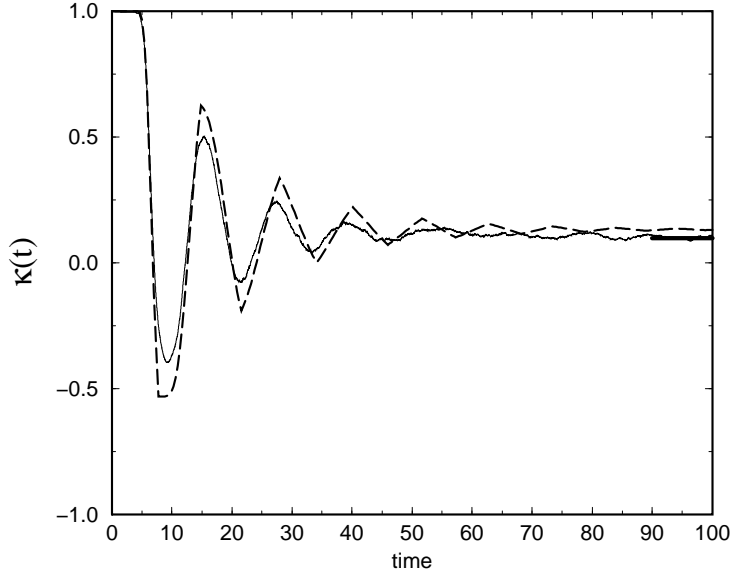


Figure 6: Transmission coefficient of an ensemble of particles at temperature  $k_B T = 0.025$  and dissipation parameter  $\gamma = 0.005$ . The particles are initially distributed above the barrier according to Eq. (37). Solid curve: simulation of 4000 particles. Dashed curve: our theory, Eq. (52), with the bare value  $\mu = 4\gamma/3 = 0.006667$ . Thick line that intersects the right vertical axis: value of the equilibrium transmission coefficient  $\kappa_{st}$  obtained from Eq. (55) using the value of  $\mu$  renormalized by thermal fluctuations, which for this temperature is  $\mu(T) = 0.004907$ .

described earlier). In other words, the drop is principally due to the particles near the top of the barrier that manage to recross. The determining features in the early time behavior of  $\kappa(t)$  are thus the time range  $0 < t < \ln(16/\mu)$ , the value of  $\mu$ , and the decay function  $f_1(t)$ . Once the least energetic particles are trapped, however, the particles of initially higher energies (although fewer in number) sequentially dominate the oscillatory behavior of  $\kappa(t)$ , that is, the higher terms in the sum become sequentially important in the time dependence of  $\kappa(t)$  as time increases. The subsequent oscillations thus reflect recrossings of the barrier. These are also captured quite accurately. The simulations and the theory settle to asymptotic values that are extremely close to one another.

The theory could of course be improved in various ways. First, the theoretical oscillations are sharper and continue for a longer time than those of the simulations because the theory

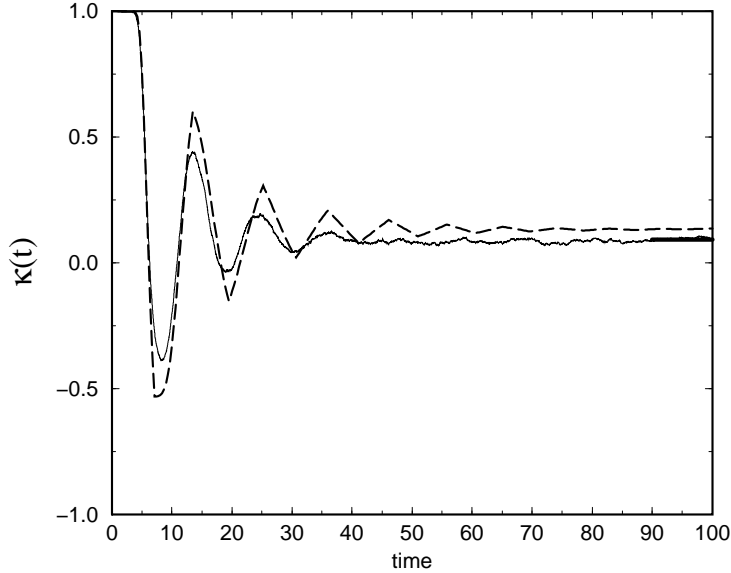


Figure 7: Transmission coefficient of an ensemble of particles at temperature  $k_B T = 0.05$  and dissipation parameter  $\gamma = 0.01$ . The particles are initially distributed above the barrier according to Eq. (37). Solid curve: simulation of 4000 particles. Dashed curve: our theory, Eq. (52), with the bare value  $\mu = 4\gamma/3 = 0.01333$ . Thick line that intersects the right vertical axis: value of the equilibrium transmission coefficient  $\kappa_{st}$  obtained from Eq. (55) using the value of  $\mu$  renormalized by thermal fluctuations, which for this temperature is  $\mu(T) = 0.007892$ .

averages or altogether ignores additional effects that lead to particle dephasing. For example, the sharp (deterministic) time cuts (which cause the sharp minima and maxima in the theory) are in reality somewhat distributed due to the fact that the particles lose energy continuously and not just at the ends of half orbits as assumed in the theory, and due to fluctuations that allow energy gains throughout the dynamics. Indeed, particles that we take to be trapped forever can in reality recross the barrier due to thermal fluctuations (but in very small numbers at low temperatures, as reflected in the small value of the equilibrium transmission coefficient). Furthermore, the average energy loss per half orbit,  $\mu(\varepsilon)$ , has been assumed independent of  $\varepsilon$ , but in reality  $\mu$  increases with  $\varepsilon$ , even in the “bare” approximation that ignores thermal fluctuations in the calculation of  $\mu$ . This dependence is contained in Eq. (28), but we have approximated the solution of Eq. (28) by the  $\varepsilon$ -independent Eq. (29), which is

an upper bound on  $\mu$ . On the other hand, thermal fluctuations contribute to a decrease in  $\mu$  as a function of temperature. Indeed, if one analyzes average energy loss trajectories such as the one shown in the middle panel of Fig. 5 but for slightly higher initial energies, one finds that there is a small upward curvature that indicates that  $\mu$  starts with the bare value but that it becomes renormalized by thermal fluctuations as time proceeds.

The theoretical equilibrium values of the transmission coefficient achieved by the dashed curves in Figs. 6 and 7 are a little higher than the simulation result. Note that the entire dashed curve in both cases has been calculated using the upper-bound bare energy loss parameter  $\mu = 4\gamma/3$ . If we rely on our result Eq. (55), the small difference between simulated and calculated results would indicate that the actual value of  $\mu$  at long times is a bit lower than the value assumed in the dashed curve. We also show in the figures the equilibrium transmission coefficient calculated in each case according to Eq. (55), but now with the renormalized energy loss parameter that follows from solving Eq. (34). For the parameters in Fig. 6 this value is  $\mu(T) = 0.004907$ , and in Fig. 7 it is  $\mu(T) = 0.007892$  (thick short lines that intersect the right vertical axis). These values of the stationary transmission coefficient agree extremely with the simulation results in both cases.

Finally, it is interesting to pursue in more detail the dependences of the equilibrium transmission coefficient  $\kappa_{st}$  on the input parameters ( $\gamma$  and  $k_B T$ ) and, in particular, to evaluate the prediction Eq. (55) for these dependences. As noted earlier, the existing results correspond to a small- $\gamma$  expansion of our result. In practically every instance that we have found in the literature, the equilibrium transmission coefficient vs dissipation parameter is drawn on a log-log plot that would mask the dependence that we are focusing on. For this analysis we return to Fig. 2 and, in particular, the low dissipation portion of the figure. We present two sets of results for  $\kappa_{st}$  vs  $\gamma$  on a semi-log plot, one for temperature  $k_B T = 0.025$  (the temperature used throughout most of this paper) and the other for  $k_B T = 0.05$ . The solid circles are the simulation results for the lower temperature, and the triangles are for the higher temperature. The first and very clear point to note is that the  $\gamma$  dependence is indeed not linear beyond the very lowest dissipation parameters. The upward curvature with increasing  $\gamma$  is clear. We then ask whether the tanh dependence in Eq. (55) captures this curvature. The only small uncertainty lies in the value of the parameter  $\mu$  to use



in answering this question. For the particular dissipation parameter value  $\gamma = 0.005$  and temperature  $k_B T = 0.025$ , and also for  $\gamma = 0.01$  and  $k_B T = 0.05$ , we have established that the equilibrium value we predict is quite accurate if we use the bare  $\mu$  and even more accurate if we use the renormalized value  $\mu(T)$ . In Fig. 2 we show the theoretical curve Eq. (55) for two temperatures using the renormalized value  $\mu(T)$ . The solid curve is for temperature  $k_B T = 0.025$ , and the dashed curve for  $k_B T = 0.05$ . Clearly the theoretical curves capture the simulation results very well over a substantial range of dissipation parameters values.

## 8 Conclusions

We have developed a theory for the time dependent transmission coefficient in the energy-diffusion limited regime of the Kramers problem. Our work complements that of Kohen and Tanner [3], whose theory covers only the diffusion limited regime. We arrive at an explicit analytic prediction for the transmission coefficient that describes the rate at which particles in the potential of Fig. 1 move over the barrier from the region associated with one well to that associated with the other. Our result depends *only* on the two input parameters of the problem, the dissipation and the temperature, and involves no adjustable parameters. For low dissipation and low temperature, our result captures the correct behavior on *all* time scales, leading to excellent agreement with simulations in the short time regime where the transmission coefficient oscillates, and also in the long time regime where it settles to an asymptotic equilibrium value. Our prediction for the equilibrium value as a function of the dissipation parameter and temperature extends beyond the regime of existing theories in this regime.

The theory starts with the Langevin equation for the system and proceeds in two stages. First, we calculate trajectory features such as the time it takes a particle to complete a half orbit and the energy loss in the course of a half orbit. This provides the ingredients that allow us to determine when particles cross and recross the barrier between one well and the other as a function of their initial energy, and how long it takes for a particle to become trapped in one well or the other. The second stage is the combination of these ingredients for an ensemble of particles that are initially distributed canonically. The resulting oscillatory

early time behavior of the transmission coefficient reflects barrier recrossing events of initially energetic particles. The equilibrium value of the transmission coefficient reflects the residual steady state flux of particles essentially trapped in one well or the other.

We also note that we have carried out new simulations in regimes where theoretical predictions were available but had not been checked, and in the regimes of interest in this paper where neither theory nor simulations were previously available. Through these simulations it has been possible for us to check our own work as well as that of others (specifically, the KT results for the diffusion-limited regime), and we now have available simulation results that can serve as a backdrop for further theoretical developments.

That a number of chemical reactions occur in the low dissipation regime has, of course long been clear, not only on the basis of theoretical considerations but on the basis of a variety of experiments (see e.g. [15, 16]). The ability to probe reactions on a very short time scale is much more recent[4, 5]. The theory we have presented provides a more complete understanding of energy-diffusion limited reactions than has heretofore been available. To further complete the picture, our work continues in order to generalize our model, most immediately to non-Markovian processes [17].

## Acknowledgment

This work was done during a sabbatical leave of J.M.S. at the University of California, San Diego granted by the Direcció General de Recerca de la Generalitat de Catalunya (Gaspar de Portolá program ). The work was supported in part by the U.S. Department of Energy under Grant No. DE-FG03-86ER13606, and in part by the Comisión Interministerial de Ciencia y Tecnología (Spain) Project No. DGICYT PB96-0241.

## References

- [1] H.A. Kramers, *Physica* **7**, 284 (1940).
- [2] For a review see P. Hanggi, P. Talkner and M. Borkovec, *Rev. Mod. Phys.* **62**, 251 (1990) and references therein.

- [3] D. Kohen and D.J. Tannor, J Chem. Phys. **103**, 6013 (1995).
- [4] See e.g. E. W.-G. Diau, J. L. Herek, Z. H. Kim, and A. H. Zewail, Science **279**, 847 (1998).
- [5] A. W. Castleman, D. E. Folmer, and E. S. Wisniewski, Chem. Phys. Lett. **287**, 1 (1998).
- [6] R. F. Grote and J. T. Hynes, J. Chem. Phys. **73**, 2715 (1980).
- [7] J. E. Straub and B.J. Berne, J. Chem. Phys. **83**, 1138 (1985).
- [8] J. E. Straub, D.A. Hsu, and B.J. Berne, J. Phys. Chem. **89**, 5188 (1985).
- [9] T.C. Gard, *Introduction to Stochastic Differential Equations*, Marcel Dekker, vol.114 of *Monographs and Textbooks in Pure and Applied Mathematics* (1987).
- [10] R. Toral, in *Computational Field Theory and Pattern Formation*, 3rd Granada Lectures in Computational Physics, Lecture Notes in Physics Vol. 448 (Springer Verlag, Berlin, 1995).
- [11] S. Adelman, J. Chem. Phys. **64**, 124 (1976).
- [12] J.A. Montgomery, Jr, D. Chandler, and B. J. Berne, J. Chem.Phys. **70**, 4056 (1979).
- [13] R. L. Stratonovich, *Topics in the Theory of Random Noise*, Vol. 1 (1963) and Vol. 2 (1967) (Gordon and Breach, New York).
- [14] K. Lindenberg and B. J. West, *The Nonequilibrium Statistical Mechanics of Open and Closed Systems* (VCH, New York, 1990).
- [15] D.L. Hasha, T. Eguchi, and J. Jonas, J. Am. Chem. Soc. **104**, 2290 (1982).
- [16] J. Troe, J. Phys. Chem. **90** , 357 (1986); J. Schroeder and J. Troe, Ann. Rev. Phys. Chem. **38** , 163 (1987).
- [17] J. M. Sancho, A. H. Romero, and K. Lindenberg, in preparation.